Tuning ceramic surface to minimize the ionic resistance at the interface between PEO- and LATP-based ceramic electrolyte

Léa Mangani, Didier Devaux, Anass Benayad, Christian Jordy, Renaud Bouchet

Tunning ceramic surface to minimize the ionic resistance at the interface between PEO and LATP based ceramic electrolyte.

*Léa R. Mangani[1], Didier Devaux[1], Anass Benayad[2], Christian Jordy[3], Renaud Bouchet[1]**

[1] Univ. Grenoble Alpes, Univ. Savoie Mont Blanc, CNRS, Grenoble INP, LEPMI, 38000 Grenoble, France

[2] Université Grenoble Alpes, CEA, LITEN, DTNM, 38000 Grenoble, France

[3] SAFT, Direction de la Recherche, 111 Boulevard Alfred Daney, F-33000 Bordeaux, France

KEYWORDS: Impedance spectroscopy, polymer/ceramic interfaces, surface composition, solid-state electrolytes, polymer electrolyte, lithium batteries.

ABSTRACT

New battery technologies are currently under development, and among them, all-solid-state batteries should deliver better electrochemical performance and enhanced safety. Composite solid electrolytes, combining solid polymer electrolyte (SPE) and a ceramic electrolyte (CE), should then provide high ionic conductivity coupled to high mechanical stability. To date, this synergy is not yet reached due to the complexity of the Li-ion transport within the hybrid solid electrolyte especially at the SPE/CE interface currently considered as the limiting step. Yet, there are no proper kinetic model to elucidate the parameters influencing this interfacial barrier. The limited understanding of SPE/CE interface can be partly explained by scattered SPE/CE interface resistances reported in the literature as well as the lack of systematic studies. Herein, we propose a systematic study of the impact on the SPE/CE interfacial resistance of chemical and thermal treatments of a model LATP based ceramic based on a methodology relying on electrochemical impedance spectroscopy (EIS) and X-ray

photoemission spectroscopy (XPS). The results provide different levers for the optimisation of this interface and valuable insights about experimental precautions needed to obtain more reproducible results.

INTRODUCTION

In contrast to organic flammable liquid electrolytes, solid electrolytes have emerged as promising candidates for the development of safer Li-ion and Li metal batteries[1, 2]. However, the substitution of liquid by solid electrolyte is far from trivial, since it requires solid electrolytes with i) sufficient ionic conductivity at room temperature, ii) electrochemical stability window compatible with electrode materials[3] and, iii) high mechanical properties to avoid positive electrode pulverization and delamination as well as dendrite growth when used with a Li metal negative electrode[4, 5].

Several classes of solid electrolyte exist, the main two being the solid polymer electrolytes (SPE) and the ceramic electrolytes (CE). SPEs possess a very favourable soft mechanical properties that lead to intimate contacts with the electroactive materials, however they have a quite low ionic conductivity that imposes to operate at elevated temperatures typically above 60°C[6]. On the other hand, CEs have a good ionic conductivity at room temperature[7, 8], but their brittleness leads to poor interfacial contacts with the electroactive materials during cycling[9]. Combining a ceramic and a solid polymer into a composite solid electrolyte could lead to a breakthrough since the benefits of each type of electrolyte maybe combined[10, 11]. However, in such composite, a new type of interfaces must be managed; the SPE/CE organic-inorganic interface that deserved a proper investigation to find the parameters controlling it.

In the literature, the interfaces formed between CE coupled with either liquid electrolytes (LE)[12-21] or SPE[22-30] have been vastly investigated since the 1990s. However, for a similar ceramic/electrolyte couple the reported interface resistances are dispersed on several orders of magnitude[31]. Therefore, it is difficult to draw a conclusion on the parameters that could lead to improve the SPE/CE interfacial resistance. The source of data dispersion could be ascribed to i) the methodology to evaluate the interfacial resistance typically by fitting and subtracting impedance spectroscopy spectra[17, 29, 30, 32, 33], and/or, ii) the sample preparation such as polymer elaboration (solvent free[34], solvent-cast[23, 29, 35, 36] processes or RF magnetron sputtering[25] in N_2 atmosphere) and ceramic pre-treatment/initial ceramic surface composition, and/or iii) the cell assembly methodology (polymer spray coating onto a ceramic[25, 29], polymer deposition by hot pressing[34]). As an example, the group of Dudney[25, 37]

demonstrated that the SPE/CE interface properties are strongly influenced by the cell assembly method as they compared two SPE/CE/SPE multilayer fabrication processes; i) polymer on ceramic and ii) ceramic on polymer. Indeed, the authors showed that the SPE/CE interfacial resistance drops significantly when the ceramic (LIPON) was directly sputtered onto the polymer layer rather than the polymer spin-coated onto the ceramic surface. Chen *et al.*[29] also reported the effect of polymer plasticizer (solvent content) on the interfacial resistance between polyethylene oxide (PEO) and a commercially available LICGC™ [38] (Lithium-Ion Conducting Glass-Ceramic, LATP-like) CE. In their work, adding TEGDME or DMC into a PEO-$LiCF_3SO_3$ polymer electrolyte resulted in a sharp drop in the interfacial resistance by 20 % and 92%, respectively[29], that was attributed to the beneficial effect of the plasticizer improving ion transport and salt dissolution near the ceramic surface. These results also suggest that there might be interactions between ceramic surface chemistry and the interfacial ionic resistance calling for further investigations.

In this work, we thoroughly investigated the interfacial resistance between a commercial LATP-like ceramic (referred as Oh, or LICGC™ [38]) and a high molecular weight PEO used as a reference solid polymer electrolyte. Three tuning routes of the PEO/CE interface were investigated i) polymer solvent plasticization, ii) solvent dip-casting of the ceramic, and iii) ceramic heat treatment. With a combination of EIS, XPS and ICP analysis, we showed that tuning the ceramic surface composition is possible and allows the significant reduction of the PEO/Oh interfacial resistance. If the PEO/Oh resistance decreases rather rapidly with ceramic surface tuning, whatever the surface treatment, they all continue to evolve over time and plateau to low values upon ageing. The present work constitutes a breakthrough in this research field, providing valuable insights into improving of solid-state batteries performance.

EXPERIMENTAL SECTION

Materials

Organic electrolytes

In an Argon (Ar) filled glovebox (H_2O, O_2 < 1 ppm, Jacomex), lithium Bis(trifluoromethane)sulfonimide (LiTFSI, Solvay) and 100 kg/mol polyethylene oxide (PEO, Alfa

Aesar) were formulated by solvent-free method. A given amount of LiTFSI and PEO were mechanically cold-mixed to reach a salt concentration of 0.5 M (EO/Li ratio) before being heated to 80 °C for at least 4 h to obtain a homogeneous mixture. The resulting PEO/LiTFSI mixture was then hot-pressed at 70 °C to form a polymer membrane. Hereafter, the polymer electrolytes are denoted as $PEO_{0.5M}$_Dry. Plasticized polymer membranes were also elaborated by the addition of a known amount of dimethylformamide (DMF) solvent to the PEO/LiTFSI mixture while being in its melted state at 65°C to ensure an uniform dispersion. The obtained membranes are denoted $PEO_{0.5M}$-*x* wt% with x = 0 wt%, 0.4 wt%, 0.6 wt%, and 2.2 wt% being the weight fraction of DMF solvent contained in the membrane and determined using ^{1}H-NMR (Bruker, 400 MHz) after cooling. To perform such NMR measurement, the plasticized polymer membranes were completely dissolved in 0.7 mL in CD_3CN, then the NMR peaks and the details about the spectrum analysis are given in **Supporting Information, Note 1 and Table S1**.

Ceramic electrolyte

Ceramic plates of LICGC™ were purchased from Ohara Corp[39] in the form of one inch squared plates with thicknesses of 150 µm. This ceramic electrolyte, denoted Oh hereafter, is similar to LATP with the main crystalline phase being $Li_{1+x+y}Al_xTi_{2-x}Si_yP_{3-y}O_{12}$. When it is not specified, ceramic is used as received and stored in an Ar-filled glovebox. The ceramic plate was also treated via solvent or thermal protocol. In the case of solvent treatment, Oh ceramics plate are fully immersed in several solvents (Dimethylformamide (DMF), Acetonitrile (ACN), Dimethyl carbonate (DMC), Sulfolane and Isopropanol) for 1 min and dry in an Ar filled glovebox for at least 3 days prior to be assembled in a cell. The ceramic thermal treatment consists of putting ceramic plate under vacuum and high temperature (different temperatures tested higher than 100°C) for a at least one-night prior being returned to the glovebox before cell assembling.

XPS surface characterization

The experiments were carried out on a Quantes ULVAC-PHI spectrometer in an ultrahigh vacuum chamber (> 7 10^{-8} mbar), using a micro-focalized mono-chromatic X-ray sources AlKα (1486.6 eV) of 100 µm diameter and 49 W. The depth of analysis is in the range of few nanometres

(~ 5 nm) and varies with the nature of core level peak as the photoelectron mean free path depends. All XPS core level binding energies were re-aligned (calibrated) using the contamination aliphatic carbon related C 1s binding energy at 284.8 eV[40], corresponding to C-C bonds. Peak fitting is performed using pseudo-Voigt function (Gaussian (70%) and Lorentzian (30%) distributions) using Casa XPS software. To prevent any contamination due to air or moisture, all samples are prepared in Ar filled glovebox and transferred from the glovebox to the XPS instrument using an airtight transfer chamber.

Cell assembly

All cells were assembled in an Ar filled glovebox (H_2O, O_2<1ppm, Jacomex). To study the interface between the SPE ($PEO_{0.5M}$) and the Oh ceramic, symmetric CR2032 coin cells comprising stainless steel blocking electrodes were assembled. The $PEO_{0.5M}$ electrolyte was flowed directly within a polypropylene spacer of 4 mm diameter onto the SS electrode using a hot press, then a piece of Oh ceramic (larger than the diameter of the polymer) is placed in between the two polymer layers. A good contact is ensured by gently pressing them together prior closing the coin cells. In the case of liquid electrolyte (PEGDME), an insulating guide/spacer with variable inner diameter and 16 mm outer diameter is placed onto SS electrodes to define the contact area between the ceramic and the electrolyte. Secondly, two pieces of Freudenberg polyolefin separator soaked with a liquid electrolyte are placed inside the spacer onto the electrodes prior putting a ceramic plate in-between. The coin cells are then sealed with a crimper before being taken out of the glovebox to carry out the electrochemical characterizations.

Impedance measurement

After assembly, coin-cells were placed in a climatic chamber (Clima Temperatur Systeme) and connected to a multipotentiostat with impedance capabilities (VMP300, BioLogic). Electrochemical Impedance Spectroscopy (EIS) measurement was performed in the frequency range of 7 MHz down to 100 mHz using an excitation voltage varying between 10 mV to 200 mV. Especially at low temperature, the input signal amplitude has been increased up to 200 mV to limit the noise while keeping the linearity of the recorded signal. In the case of SPE, the climatic chamber temperature

varied from -30 °C to 100 °C following a temperature program: i) first heating from room temperature (RT) to 100°C by step of 20°C and 1 h of thermal equilibrium is performed for each temperature, ii) second cooling down to -30°C, by 5 °C steps in between 100 °C and 60 °C, and then by 20 °C steps below 60 °C, iii) final heating up to 100 °C by 20 °C steps. The cells were then stored at RT before being placed again in the climatic chamber to follow the evolution of cell impedance over ageing time and using similar temperature program.

In addition, we evaluated the experimental error on PEO/Oh resistance and corresponding E_a based on reproducibility experiments performed using similar polymer membranes and ceramic pieces cut from the same ceramic plate. We evaluated an uncertainty below 15%.

ICP characterization

Inductively Coupled Plasma Mass Spectroscopy (ICP-MS, PerkinElmer NexION 2000c) was used to study the effect of solvent immersion on ceramic plate. At first, Oh ceramic is immersed for 20 h in a known volume of ACN, DMF solvent or deionized water in an Ar filed glove box. Second, the solution is analysed to possibly detect the presence of chemical elements that could have been leached (Li, Al, Si, P, Ti, Ge and O) from the ceramic. It is worth mentioning that ICP detection accuracy limit is around 0.5 ppb and knowing the molar mass of Li, Al, Ti and Ge element, its means that below 10^{-7} $g/g_{Oh\ piece}$ (comparing the threshold mass detected to the total mass of the immersed piece of ceramic), only traces of chemical element are detected (concerned values are highlighted in italics in **Table 1**). Additionally, to improve the accuracy of the results given in **Table 1**, concentrations are also corrected from the residual traces of Li, Ge, Al and Ti detected in empty tests tubes and measured separately (ICP quantification performed using deionized water in an empty vial used as received).

RESULTS AND DISCUSSION

To investigate the effect of sample preparation onto the interfacial resistance of PEO/Oh several parameters were tuned i) SPE was elaborated via solvent-free method with and without solvent addition, ii) the CE was either used as received or pre-treated (thermally or via solvent-treatment) as

described in the experimental section. Based on our methodology detailed in our previous work[41], PEO/Oh interfacial resistance was measured at different temperatures to extract the activation energy. More specifically and as can be seen in **Supporting Information Figure S1**, the PEO/Oh interface impedance are assigned to the MF semi-circle denoted as R_{ion}/CPE_{ion} and associated to Li-ion transport trough the interface. The recorded results are gathered in **Figure 1** and showed that there is a strong impact (up to a factor 7) on R_{ion} when varying polymer or ceramic preparation protocol.

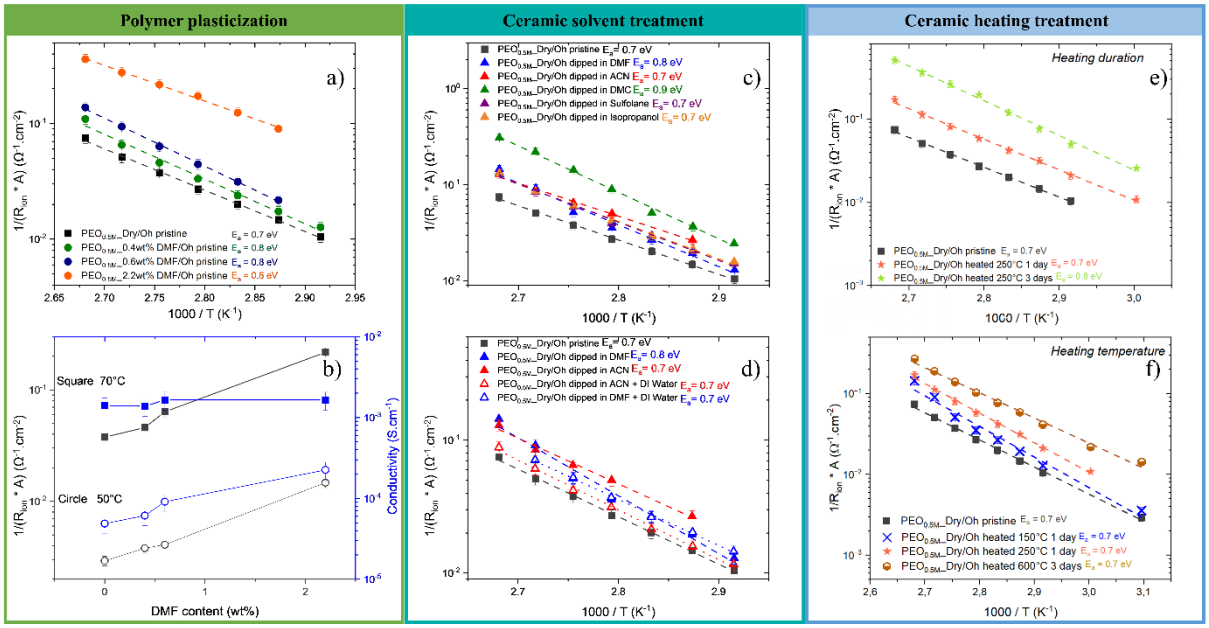

***Figure 1**. a), c), d), e) and f) Arrhenius plot of R_{ion} measured at Oh/$PEO_{0.5M}$-xwt%, at $Oh_{dipped\ in\ solvent}$/ $PEO_{0.5M}$_Dry and at Oh_{heated}/ $PEO_{0.5M}$_Dry compared to reference $Oh_{pristine}$/$PEO_{0.5M}$_Dry. b) Evolution of the inverse of the interfacial resistance of Oh/$PEO_{O.5M}$_Dry-x and plasticized polymer bulk ionic conductivity at 70°C and 50°C, respectively, as function of DMF solvent, recorded 2 h after cell assembly.*

1- Impact of polymer solvent plasticization

At first, we investigated the variation of R_{ion} when varying PEO polymer solvent plasticization amount. DMF solvent was added with the following amount 0.4 wt.%, 0.6 wt.% and 2.2 wt.% to a $PEO_{0.5M}$-LiTFSI (solvent-free elaborated) SPE (DMF solvent quantification in **Table S1**). In **Figure 1a,** Arrhenius type plot is displayed and shows that R_{ion} decreases linearly with the temperature from which the activation energy, noted as E_a, can be extracted. At 30°C, an interfacial resistance of

3.4 kΩ.cm² is found for $PEO_{0.5M}$_Dry(LiTFSI)/Oh interface which is in to the range of value reported in our previous works[41, 29] using similar polymer and ceramic materials (varies from 1.2 to 2.6 kΩ.cm²). When adding DMF residual, R_{ion} decreases significantly up to a factor of 6 for the sample containing 2.2 wt.% of DMF compared to the dry sample. This finding suggests that residual solvent drastically reduces R_{ion} (hence, fasten the interfacial ionic transport kinetics) which can be the first source of data scattering in the literature. As an example, Chen *et al.*[29] reported values drastically lower than our dry sample for $PEO_{1.3M}$_solvent casted(LiTf)/Oh interface which could be linked to solvent residual (in their case DMC) that facilitates ion transport and Li cation dissociation near the ceramic interface.

In addition, we investigated the impact of DMF content onto the ionic conductivity of polymer electrolyte at 70°C and 50°C ($T < T_m$) in **Figure 1b**. Above the melting temperature, there is almost no impact of solvent residual onto the ionic conductivity. More precisely, the ionic conductivity is constant while $1/R_{ion}$ increases linearly in this coordinate (*i.e.* a power law) with the DMF content in **Figure 1b**. This suggests that even a residual solvent in the SPE significantly impacts R_{ion}. Below T_m, a significant enhancement of the bulk conductivity is also noticed in line with the decrease of crystallinity induced by the solvent traces[42-44].

Regarding E_a, it slightly increases with the addition of DMF content from 0.7+/- 0.1 eV for the dry SPE to 0.8+/- 0.1 eV for PEO_0.4 wt%, except for PEO 2.2 wt.% of DMF that showed an E_a value of 0.6+/- 0.1 eV. E_a values lie in the same order of magnitude which indicates that the ionic transfer mechanism remains the same. Therefore, the addition of a small amount of solvent in a SPE appears to be a simple and effective strategy to minimize the SPE/CE interfacial resistance. It is worth mentioning that the addition of solvent or plasticizer may impact negatively other battery components, as an example, DMF and ACN are known to be unsuitable with Li metal electrode[45, 46]. In addition, the variation of the interfacial capacitance associated to PEO/Oh interface with polymer solvent content is displayed in **Figure S2a**. There is a limited impact of polymer solvent content on C_{ion} but we observe a slight increase with solvent content up to a factor of 1.4 for 2.2wt% DMF compared to the reference. In addition, the increase of the interfacial capacitance C_{ion} seems to be correlated with the decrease of

R_{ion} (the lower $R_{ion,}$ the larger C_{ion}).[47] ~~This coordinated variation indicates that solvent addition result in the increase of SPE/CE space charge layer which enable faster interfacial Li ion transport.~~

2. Ceramic solvent treatment

Based on the previous investigation from solvent residual effect onto the SPE/Oh interface, we investigated the impact of direct treatment of the ceramic surface by solvents. But prior starting, we verified that the bulk of the ceramic was not significantly impacted by the solvent treatment following the methodology presented in our previous work[41]. We also assessed that the HF overall resistance of the multilayer cells (R_{HF}= 2 R_{PEO} + R_{Oh}) well corresponds to the algebraic sum of the bulk resistance of the PEO and Oh layers (**Figure S3**). Additionally, we tested first the impact of dipping the ceramic onto water to ensure that the effect recorded with organic solvent are not linked to a residual water content. In the specific case of water, R_{ion} at Oh/PEO is not modified which is in line with supplier information indicating that ceramic is not water sensitive since a water-based solution is used during ceramic shaping procedure (See **Figure S4).**

In **Figure 1c**, we show the Arrhenius plot of the R_{ion} measured for $PEO_{0.5M}$_Dry with a ceramic preliminary treated with different solvents (ACN, DMF, sulfolane, DMC, isopropanol). As can be seen, surface ceramic treatment by solvents causes a similar reduction of R_{ion} as it was observed for solvent plasticized polymer (**Figure 1a**). Compared to the pristine $PEO_{0.5M}$_Dry/Oh, the dipping process of the ceramic lowers R_{ion} by 25%, 50% and up to 65% for DMF, ACN and DMC solvent, respectively, showing that this simple method is very effective for reducing R_{ion}. We also recorded the variation of R_{ion} when the ceramic is dipped into successive solvents. **Figure 1d** displays the Arrhenius plot of the interfacial resistance when the ceramic was initially soaked in either DMF or ACN and then in deionized water (DI). For DMF followed by water, R_{ion} is similar to that of reference Oh_{DMF}/$PEO_{0.5M}$_Dry. However, for ACN followed by water, R_{ion} is slightly higher compared to $Oh_{in\ ACN}$/$PEO_{0.5M}$_Dry but remains 14% lower on average than the pristine ceramic interface. The latter

result suggests that subsequent soaking in water seems to mitigate the effect of the initial soaking in the case of ACN pre-treatment.

Except for $PEO_{0.5M}$_Dry/$Oh_{in\ DMC}$ interface, the E_a is only slightly affected by the ceramic solvent pre-treatment (**Figure 1** legend) which suggests that Li-ion transport mechanism through the PEO/$Oh_{treated}$ interface remained unchanged.

The interfacial capacitance (C_{ion}) at $PEO_{0.5M}$_Dry/Oh interface appears to increase when the ceramic is preliminary dipped in solvent (**Figure S2b**). Interestingly, the highest C_{ion} were measured for ACN and DMC solvent treatment for which we record the lowest R_{ion}. This finding suggests that the surface composition and defect chemistry which impacts the space charge layer, probably vary after ceramic surface treatment and lead to higher kinetics for the Li ion transport across the interface. In addition, it supports the idea that the dominant capacitance at PEO/Oh settled on the ceramic side as already discussed in our previous work[41] in which PEO_{xM}/Oh interfacial capacitance was found to not vary with polymer salt concentration.

3. Ceramic thermal treatment

If in the first sections we investigated the impact of solvent treatment, another efficient technique might be to apply heat treatment coupled to vacuum (10^{-2} mbar) onto the ceramic. Hence, R_{ion} is measured using dry PEO polymer and a thermally pre-treated ceramic (**Figure 1e and f**). R_{ion} is reduced for pre-heated ceramic, in average, by 54 % and 84 % for 1 and 3 days thermal treatment, respectively. When the temperature treatment increases from 150°C to 600°C (see **Figure 1e and f**), R_{ion} seems to further decrease, calling for thermal treatment protocol optimization. The E_a is only slightly affected by the thermal treatment of the ceramic, since we found E_a constant (0.7 eV) when Oh is heated at 250°C for 1 or 3 days at 250°C compared to the reference.

It is worth noticing that similarly to the SPE solvent residual and ceramic solvent treatments, the interfacial capacitances C_{ion} (**Figure S2 c**) of heat-treated samples increase, herein up to 3-fold compared the reference sample, in correlated manner with the decrease of R_{ion}, which confirm the reliability of these results. The variations of C_{ion} suggest an increase of the charged defect content in

the extreme surface of the ceramic caused by the thermal treatment which, in turn, may facilitate the Li ion transport through the PEO/Oh interface.

Whatever the treatment applied (polymer plasticization, ceramic solvent, or heat treatment), it affects the interfacial Li-ion transport kinetic constant while the activation energy is quasi constant, leading to a decrease of R_{ion}.

At this stage, the 3 days-lasting ceramic heat treatment seems to be the most efficient way to reduce R_{ion} (a factor of 6) and since no chemical is present in the system, it would preserve the battery from additional side effects. However, during ageing the results might not be similar since the ceramic surface composition can further evolves, impacting again the R_{ion}. This aspect is discussed later in the paper. Therefore, these results provide a major advance in the understanding of the dispersion sources of measured SPE/CE resistance and call for greater attention to material preparation protocol for both polymer and ceramic[48, 49].

5. Evolution as a function of time

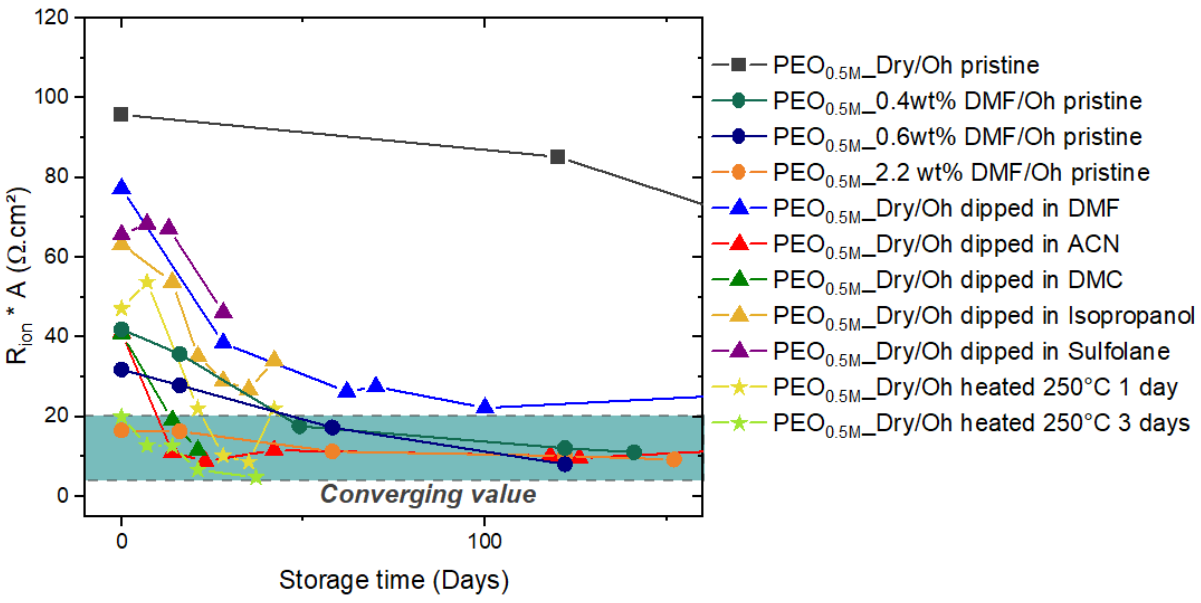

***Figure 2**: Evolution with time of the interfacial resistance Rion measured at 70°C for the different Oh/PEO interfaces.*

As discussed, R_{ion} could still evolve with time due to the ongoing chemical modification of the PEO/Oh interface as reported in the work of Busche *et al.*[13]. The evolution of R_{ion} at 70°C as function of time-storage (ageing) is displayed in **Figure 2**. R_{ion} for solvent-free polymer remains stable compared to the other samples that showed a decrease over time before stabilizing after ca. 2 weeks. In the case of polymer solvent plasticization or ceramic solvent treatment, the time evolution of R_{ion} may suggest that there is a slow equilibrium between solvent traces and ceramic and/or polymer at Oh/PEO interface. Similarly, **Figure 2** shows that ceramic heating treatment leads to a decrease of R_{ion} with time but with a faster stabilisation reaching about 10 Ω.cm² after a couple of days only. Whatever the treatment (polymer plasticization, ceramic solvent, or heat treatment) in **Figure 2**, R_{ion} values are significantly reduced over ageing time and tend to a range of values from 5 to 20 Ω.cm², at 70 °C with an activation energy of 0,7 +/-0,05 eV. This suggests that all ceramic pre-treatments and polymer plasticization affect the interfacial Li-ion transport kinetics, but the stabilization period (time to reach an equilibrium value) as well as the value depends on the sample preparation protocol. In addition, the decrease and stabilisation of R_{ion} over ageing time is synchronised with the increase and stabilisation of the interfacial capacitance C_{ion} [47] as displayed in **Figure S5**.

A similar ageing behaviour of SPE/CE resistance has been reported in the work of Gupta[50], with an initial R_{ion} decreasing period followed by a growth. Busche *et al.*[13, 51] described a temporal evolution of R_{ion} at the interface between Oh or LIPON with Dioxolane or Dimethoxyethane based electrolyte reaching an equilibrium due to the formation of an interphase made of decomposition products coming from salt, solvent, and CE typically in a couple of hours. Interestingly in their work, as in our, the delay to reach stabilisation depends on the electrolyte nature. However, herein a dozen of days is needed for R_{ion} stabilization when using solvent treatment, probably because of the low concentration of solvents within the SPE.

Understanding the role of solvent and thermal treatment

Element leaching investigated by ICP

X-ray diffraction was carried out on the treated ceramics and compared to the pristine ceramic to ensure the bulk structure is not affected. As can be seen in **Figure S6**, the solvent did not modify the bulk structure of the material, indicating that if a chemical reactivity exists, it only occurred at the surface of the ceramic.

We, further analysed by ICP-MS the solvents after ceramic immersion for 20 h and quantified relevant elements concentration as displayed in **Table 1**.

Table 1. *Chemical elements detected in ACN and DMF residual solution after ceramic immersion using ICP-MS technique (~~shaded table cells~~ values in italic and grey fonts are close to the ICP-MS detection limit).*

Samples	Li [$g.g^{-1}_{Oh\ piece}$]	Ge [$g.g^{-1}_{Oh\ piece}$]	Al [$g.g^{-1}_{Oh\ piece}$]	Ti [$g.g^{-1}_{Oh\ piece}$]
Oh dipped in 3 mL of **ACN** for 20h	$3.65\ 10^{-7} \pm 0.07$	*$2.69\ 10^{-8} \pm 0.05$*	$3.41\ 10^{-7} \pm 0.07$	*$4.9\ 10^{-8} \pm 0.7$*
Oh dipped in 3 mL of **DMF** for 20h	$1.82\ 10^{-5} \pm 0.04$	*$1.63\ 10^{-7} \pm 0.03$*	$1.73\ 10^{-6} \pm 0.03$	*$1.5\ 10^{-7} \pm 0.2$*
Oh dipped in 0.1 mL of **Water** for 20h	$6.4\ 10^{-6} \pm 0.1$	$1.40\ 10^{-6} \pm 0.08$	$2.55\ 10^{-7} \pm 0.05$	(not measured)

The solvent dipping procedure is not chemically neutral since several elements are detected and their extent depends on the solvent employed. Interestingly, we recorded a larger amount of ceramic metal ion leaching in the case of DMF compared to ACN solvent for which the amount detected is close to the limit of detection. This finding suggests a certain chemical affinity between Oh ceramic surface and DMF solvent which cannot be correlated to the water content (leading to lithium/proton exchange [52]) in the solvent since we recorded, using Karl Fisher titration, a lower water content in DMF compared to ACN, with 25 ± 3 ppm and 40 ± 3 ppm water content, respectively. At this stage, the leaching of several elements, in addition to the Li, indicates that the solvent is not only interacting physically with surface native layer[51] (*e.g.* LiOH and Li_2CO_3) but also chemically even if the dissolution is rather minimal. The Li quantity detected hints for Li coming from the surface of the ceramic since i) the carbonate is not very thick as suggested by XPS data, and ii) the quantity detected with DMF solvent (ca. 2,75 ppm) is significantly larger than the reported solubility of lithium carbonate in DMF (0.3 ppb)[53]. The latter finding is in line with the small change in ionic conductivity

recorded for solvent treated ceramic plate compared to pristine sample (**Figure S3**). Besides, this finding further confirms that the diminution of R_{ion} at $Oh_{modified}$/PEO is related to a modification of ceramic surface composition and not to its bulk properties. For the other elements, like Ti, Al and Ge, it goes in the direction of surface chemistry modification.

XPS investigation

All samples that were chemically modified (solvent procedure) and the one heat treated were carefully investigated by XPS analyses. The typical XPS survey of Oh pristine is displayed in Supporting Information (**Figure S7**) along with the LiCGC© chemical formula.

The XPS high resolution spectra of carbon (C 1s), oxygen (O 1s) of Oh pristine and treated samples are displayed in **Figure 3**. The XPS spectra related to titanium (Ti 2p), phosphorus (P 2p) and silicon (Si 2p) are given in **Figure S8**.

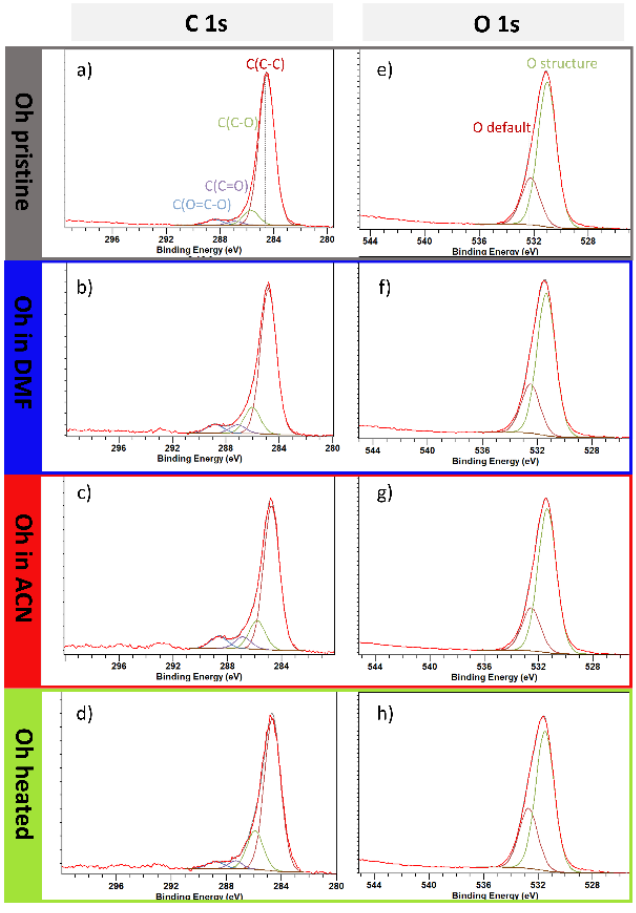

Figure 3*. XPS high resolution spectra of carbon C 1s and oxygen O 1s of Oh ceramic samples: pristine (a and e), solvent treated in DMF (b and f) and ACN (c and g) (soaked for 1 min), or thermally heated at 250°C for 3 days (d and h), respectively.*

Figure 3 a-d compares the C 1s core level spectra of samples that can be deconvoluted into 4 bands: alkyl carbonate or semi-carbonate (referred as O-C=O) at ca. 288.9 eV, carbonyl or polymeric species (referred as C=O) at ca. 287.5 eV, alkoxide or

carboxylate compounds (referred as C-O) at ca. 286.8 eV, and finally, the major contribution assigned to aliphatic carbon (referred as C-C or C-H) of contamination at ca. 284.8 eV (used as calibration peak) as detailed in **Figure 3a**. The C 1s recorded spectra are in agreement with reported works on similar ceramic material exposed to air and moisture [47, 51,54].All samples display the same four contributions, but their proportion differs depending on the surface treatment applied. As a direct comparison between C 1s core level spectra between samples is not possible (without a stable reference peak), we compare the overall contribution of carbon species (sum of area of the different bands in the C 1s spectra) to the one of a chemical element present in Oh structure, *i.e.*, Ti and P. The ratio between C to Ti and P is displayed in **Table 2**. A significant decrease of both ratios (C/Ti ratio and C/P) is noticed with the following trend Pristine > $Oh_{in\ DMF}$ > $Oh_{in\ ACN}$> Oh_{Heated} in agreement with R_{ion} evolution displayed in **Figure 1**. It indicates that the solvent treatment and the temperature treatment reduce the carbon content at the ceramic surface leading to fasten Li ion transport through Oh/PEO interface.

Table 2. Atomic concentration ratio estimated from Ti 2p, P 2p, Si 2p and O 1s and C 1s core level spectra fitting results.

Sample		**Oh pristine**	**$Oh_{in\ DMF}$**	**$Oh_{in\ ACN}$**	**Oh_{Heated}**
R_{ion} at 70°C after stabilisation [Ω.cm^2]		64	27	14	5
Carbon element	%At C/Ti ratio	29.5	23.0	20.0	18.5
	%At C/P ratio	2.1	1.5	1.4	1.2
Oxygen element	%At O/Ti ratio	35	41	39	43
	%At O default/O structure ratio	0.33	0.35	0.3	0.43
Ti element	%At Ti (IV)	91.2	88.2	87.6	90.9
	%At Ti (III)	8.8	11.8	12.4	9.1
	%At Ti (III)/%At Ti (IV) ratio	0.10	0.13	0.14	0.10
Si element	%At Si/O ratio	0.03	0.03	0.03	0.01

For the O 1s core level spectrum, displayed in **Figure 3 e-h**, the asymmetry of the peak shows several contributions attributed to ceramic network oxygen, oxygen-based surface compounds (e.g. carbonate) and ascribed to sub-oxide non-stoichiometric oxygen bonded atoms such as structural surface defect (e.g. vacancies) and/or hydroxyl compound adsorbates. Only one component will be used to describe the bulk and surface based oxygen (referred as “O default"), since the energy

resolution of the spectrometer (0.7 eV) does not allow differentiating both component. The variation of oxygen species relatively to Ti concentration for each ceramic treatment was calculated and the results are given in **Table 2**. No clear correlation was found between O 1s core level spectra variation and the recorded R_{ion} since $Oh_{pristine}$, $Oh_{in\ DMF}$ and $Oh_{in\ ACN}$ have roughly the same ratio of default/structure oxygen, which is not the case for thermally treated sample. This finding suggests a different surface modification mechanism in the case of ceramic thermal treatment compared to the solvent one. Still, the variation in the O 1s core level peak asymmetry may be related to the variation of carbonate superficial layer and/or could witness a modification of the oxygen environment. Indeed, ICP measurements reveal that some transition metal cations have been leached during solvent treatment which might lead to the formation of cation vacancies, or cation segregation resulting in oxygen environment modification at the ceramic extreme surface. The resulting ceramic structural surface modification, including surface defects may result in the modification of the surface ionic conductivity of the ceramic as pointed out by Adachi *et al.*[55] and of Yamada *et al.*[56]. In the later work, the authors reported an increase in Li_2SiO_3 coated LATP ceramic conductivity thanks to the formation of a beneficial space charge layer at LATP/ Li_2SiO_3 interface which compensates for the initial lithium depletion in the LATP pristine surface.

In agreement with the presence of Ti (+IV) in Oh structure, Ti $2p_{3/2}$ and Ti $2p_{½}$ core level spectra are observed in **Figure S8** at 459 eV and 465 eV, respectively. For clarity, only the Ti $2p_{3/2}$ core level spectrum is analysed in **Figure S8**. However, the peak presents an asymmetry towards lower binding energies requiring an additional component to minimize the fitting residue. This asymmetry suggests an apparent reduction of a small proportion of Ti(IV) into Ti (III). Indeed, Ding *et al.*[57] reported similar variation in Ti 2p core level spectrum and assigned the asymmetrization to the reduction of Ti(IV) into Ti(III) resulting from the thermal treatment of Oh ceramic under quite reducing Ar or vacuum atmosphere. The fitted peak areas are gathered in **Table 2**. Both total at% of Ti and peak asymmetry (associated to the relative at% of Ti(III) related to Ti(IV)/Ti(III) ratio) follows the trend $Oh_{in\ ACN} > Oh_{in\ DMF} >$ Oh pristine ≈ Oh_{Heated}. Due to rather noisy spectra, it is difficult to conclude on a direct link between R_{ion} and the Ti core spectrum. Still, the partial reduction of Ti(IV) into Ti (III)

leads to a change in the electron density around the d orbital of the titanium (from d0 to d1), which could affect the charge compensation around the PO_4 polyhedron and in turn, induce a variation in the local diffusion/transport kinetics. The latter variation may explain the recorded decrease of R_{ion} especially in the case of solvent treated ceramics.

The P 2p spectra show an asymmetry toward higher binding energies which can be assigned to a local change of the charge compensation around phosphorous polyhedron. This variation could be due to the presence of defected polyhedron "PO_{4-x}" and/or to trivalent aluminium causing lithium deficiency in the vicinity of $AlPO_4$ impurities (**Figure S6**). In literature, Yamada *et al.*[54] reported an Al and Li-rich surface layer (segregation) in pristine Oh ceramic after being etched by ionic beam over a depth up to 147 nm, but did not observe any change in Ti or P content. They explained such segregation by the redistribution of defects at ceramic surface, which can be similar to our observation.

Regarding the silicon signal, we noticed a singular behaviour of Oh_{heated} sample. We did not record a significant variation in the Si/Ti or Si/O ratio in the case of Oh_{inDMF} or $Oh_{in\ ACN}$ samples compared to the reference sample. However, Oh_{heated} showed an increase for both ratios suggesting a specific segregation of silicon element and/or a depletion of other chemical elements at ceramic surface.

Pursuing our investigations, we calculate the relative variation of cation/anion (Ti, P, Ge, Al)/O ratio for the different samples as shown in **Figure 4**. The fitted peak area and corresponding atomic concentration are given in **Table S2**.

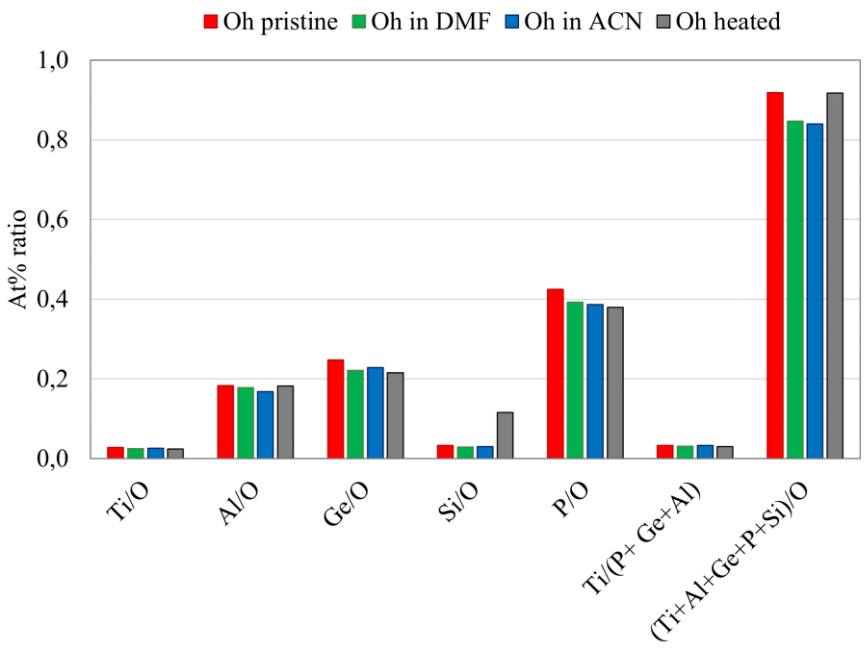

Figure 4*. Atomic concentration (%) of XPS core level peaks fitted area of different ceramic surface samples along with b) their corresponding ratio.*

In the case of Al and Ge element, the at% are based on the fitting of all the different bands identified in Ge 2p and Al 2p spectra. The ratio cation/O remains constant for Ti and Al while it decreases for Ge and P elements for treated ceramic compared to reference sample. In particular, we notice a segregation of Si element at the extreme surface in the case of Oh_{Heated} sample to form silicate rich phase which is in line with the reported results of Yamada *et al.*[54]. In addition, Oh_{Heated} sample showed a similar (Ti+P+Al+Ge+Si)/O ratio as the one of pristine sample while solvent-treated ceramic showed a decrease that might suggest a depletion of cation and/or a segregation of oxygen vacancies at ceramic surface. Therefore, we can see a different behaviour between the solvent treated samples and the heat-treated sample. Both show a decrease in R_{ion}, but the surface investigation tends to indicate that the mechanisms behind is not similar. For the heat-treated sample, it seems that the carbonate was removed from the surface, whereas for other solvent treated samples, a modification of surface chemistry (partial reduction of Ti) is more likely to reduce R_{ion}. Besides, the ratio Ti/(P+Ge+Al) recorded for treated ceramic are similar to the one of pristine ceramic surface which suggests a limited depletion of cation at the ceramic extreme surface. This finding is in line with the recent work of

Castro *et al.*[58], reporting no significant change in Ge, Al and P signals when Oh ceramic was immersed in carbonate-based solvent.

***Post-mortem* investigation of ceramic plate after contact with polymer electrolyte**

We also recorded the post-mortem XPS spectra of Oh $_{modified}$/PEO$_{1M}$-Dry samples by taking the ceramic plates out from the SPE/Oh/SPE multilayer cell assembly after recording R_{ion} and its stabilization period (*ca.* more than 2 weeks ageing). The samples are denoted Oh $_{Heated}$/PEO$_{1M}$-Dry, Oh $_{in\ ACN}$/PEO$_{1M}$-Dry when using ceramic preliminary heated or dipped in ACN solvent, respectively. In the case of Oh $_{Heated}$/PEO$_{1M}$-Dry sample, XPS spectra displayed in **Figure S9** shows additional signals caused by the presence residual electrolyte film at the top of the ceramic and made of polymeric chain and lithium salt residues. The characteristic binding energies of the fluorine and the sulfur elements are consistent with reported XPS spectra of LiTFSI salt [59]. **Figure 5** displays the corresponding high resolution XPS spectra of carbon (C 1s), oxygen (O 1s), ~~titanium (Ti 2p), phosphorus (P 2p),~~ fluorine (F 1s) and sulphur (S 2p).

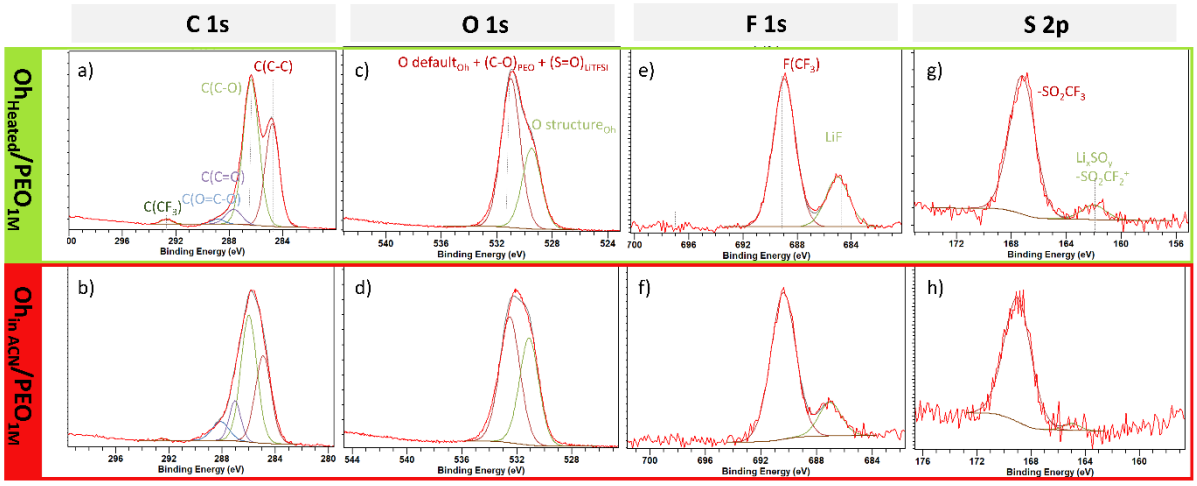

Figure 5. *XPS high resolution spectra of a-b) carbon, c-d) oxygen, e-f) fluorine and g-h) sulphur of post-mortem Oh ceramic samples that was initially thermally heated at 250°C for 3 days or solvent treated in ACN (soaked for 1 min) prior being put in contact with PEO$_{1M}$-LiTFSI in a symmetric coin cell assembly for ca. 3 weeks, respectively.*

Based on **Figure 5**, there is a significant variation in C 1s and O 1s core spectra for post-mortem samples compared to pristine ceramic sample. The variation observed are mainly related to the

signal of the residual LiTFSI doped polymer film that stays on the top of the ceramic. In **Figure 5a**, we can clearly distinguish the characteristic band of CF_3 bounds ascribed to the presence of TFSI anion at the surface of Oh_{Heated}/PEO_{1M}. From the C 1s core spectra of Oh_{Heated}/PEO_{1M}, no significant variation in LiTFSI-doped PEO signal is observed whereas we noticed a drastic change in the carbon based structure in the case of $Oh_{in\ ACN}/PEO_{1M}$ sample. Those variations could be mainly assigned to the PEO polymer backbones modification such as a local polymer plasticization close to the ceramic surface. The singular stability of PEO_{1M} in contact with Oh_{heated} might be enabled thanks to the presence of a SiO_2 rich passive layer at the ceramic surface as observed on Oh_{heated} ex-situ sample (in **Table 2**) which may protect the polymer from decomposition and provide a faster interfacial ionique transport (i.e. smaller R_{ion}).

The evolution of Ti 2p core level peak asymmetry is given in **Table 3**. It is increasing for post-mortem samples compared to their respective reference which suggests that the Ti is further reduced once in contact with LiTFSI doped PEO (Dry), but the mechanism leading to this observation is unclear yet. Similarly to the ex-situ sample, the partial reduction of the Ti can induce a variation in the charge compensation around the PO_4 polyhedron and thus affect the local diffusion/transport kinetics (cationic distribution).

***Table 3**. XPS core peaks of Ti 2p, P and C bands fitting result.*

Sample	%At Ti (IV)	%At Ti (III)	%At Ti (III)/%At Ti (IV) ratio	%At P/S(TFSI)	%At P/C(C-O)
Oh pristine	91.2	8.8	0.10		
$Oh_{in\ ACN}$	87.6	12.4	0.14		
Oh_{Heated}	90.9	9.1	0.10		
$Oh_{in\ ACN}/PEO_{1M}$	80.8	19.2	0.24	7.3	0.4
Oh_{heated}/PEO_{1M}	84.5	15.6	0.18	2.9	0.2
Ratio decrease				*2.5*	*2*

However, in the case of post-mortem sample, the recorded XPS signal account for the signature of the residual polymeric layer whose thickness is not controlled and may varies between samples, which can affect the element core level spectra intensity. Therefore, the comparison of P/S(TFSI) and P/C(C-O)

atomic concentration ratio is an undirect way to compare the thickness of the polymeric residual layer between the post-mortem samples. Based on **Table 3**, it comes that the residual polymer layer thickness is larger in the case of Oh_{Heated}/PEO_{1M} that is consistent with the observation of C 1s and S 2p spectra in **Figure 5** with a more "intense" signature of polymer+salt for the Oh_{Heated}/PEO_{1M} sample.

Figure 5 e and f show the XPS spectra in the F 1s region with a peak at 688.8 eV corresponding to the energy of C-F bonds coming from LiTFSI (CF_3) and another one at 685 eV assigned to LiF[59]. The intensity of LiF signal varies between the samples with a larger proportion for Oh_{Heated} which is assigned to the variation of the residual uneven polymeric layer. The LiF signature also suggests the decomposition of TFSI anion on the surface of Oh ceramic[47, 51] as reported by Busche *et al.*[51] on a DOL:DME-LiTFSI/Oh and LIPON surface and by Vivek *et al.*[47] on Oh surface using wet (5 wt% water) DOL:DME-LiTFSI electrolyte. Moreover, Li salt decomposition is further supported by the S 2p core level spectrum (**Figure 5 g and h**). It displays a large peak at 167 eV that corresponds to $-SO_2$ in TFSI and an additional peak at ca. 161 eV ascribed to the presence of some sulfone/sulphide fragments that result from anion decomposition at the ceramic surface[60]. In situ XPS experiments should help to get further insights on the interfacial compounds generated at the interface between Oh/PEO and therefore help to optimize ceramic surface treatment to minimize R_{ion} especially regarding the partial reduction of Ti or the formation of a SiO_2 rich layer.

CONCLUSION

We report that R_{ion} at PEO/Oh can be modified by residual solvent trapped in the SPE, even at levels where the SPE plasticization effect on ionic conductivity is barely noticeable (below 5 wt%). For instance, R_{ion} is reduced by a factor of 6 with only 2.2 wt% of DMF in polymer. The presence of residual solvent also causes a significant decrease of R_{ion} over time until reaching a plateau after few days/weeks, a phenomenon not observed for solvent-free SPE. Such results suggest that the R_{ion} data reported in the literature should be taken with precaution. This finding also implies that R_{ion} at Oh/PEO can be controlled. A demonstration has been given using Oh dipped in solvents (for 1 min) or heated under vacuum at 250°C for 3 days, which result in a drop of R_{ion} of more than a decade. We find out, using XPS coupled with XRD, that ceramic treatment induces a change in extreme surface

composition (2-5 nm) with a decrease of the surface carbon contamination content and a segregation of cations (Ti, Ge, P and Si) to form cation-rich surface layer coupled with the partial reduction of Ti element. In the case of thermal treatment, XPS experiment might show Si-rich phase formation at Oh extreme surface. Interestingly, these surface modifications result in the increase of PEO/Oh interfacial kinetic constant up to a factor of 10, since the E_a was not modified by ceramic treatments. Additionally, the temporal evolution of R_{ion} coupled with XPS *post-mortem* analyses suggest a reactivity of the anion and polymer chain with Oh surface as evidenced by the presence of LiF and Li_2S (reduction of $TFSI^-$). Interestingly, this reactivity seems exalted with pre-treated ceramic and correlated to the extent of R_{ion} drop.

ASSOCIATED CONTENT

Supporting Information. Equation of polymer solvent content determined by NMR technique, Nyquist plot of model SS/SPE/CE/SPE/SS multilayer cell impedance along with its equivalent circuit, thermal behaviour of interfacial capacitance of CE/SPE interface, Arrhenius plot of CE conductivity measured from SS/SPE/CE/SPE/SS multilayer cell impedance spectra, Arrhenius plot of CE/SPE ionic resistance using a water-soaked ceramic, ageing of CE/SPE interfacial capacitance, XRD patterns of pristine and treated ceramic powder, XPS survey and core lever spectra of Ti, P and Si along with spectra fitting data of pristine and treated ceramic samples.

AUTHOR INFORMATION

* Email : renaud.bouchet@grenoble-inp.fr

Author contributions

L.R.M. and R.B. conceived the idea and designed the experiments. L.R.M. carried out the sample preparations, performed the experiments and data treatments with the support of RB, DD and AB. A.B. performed the XPS measures. All the authors contributed to the data interpretation. L.R.M., D.D. and R.B. cowrote the paper. R.B. and C.J. got the financial support. All authors discussed the results and commented on the manuscript.

Funding Sources

The SAFT company and the Association Nationale de la Recherche et de la Technologie (ANRT) are acknowledged for their financial support through the CIFRE contract N° 2019/1133. In addition, the Agence de la Transition Ecologique (ADEME) is also acknowledge for the funding through the project IDOLES N°1982C0016.

AKNOWLEDGMENT

The authors thank Dr. James A. Isaac (LEPMI) for the NMR experiments, Mr. Vincent Martin (LEPMI) for the help with ICP-MS analysis and Dr. Stéphane Coindeau (CMTC, advanced characterization platform of G INP) for the XRD experiments.

REFERENCES

(1) Janek, J.; Zeier, W. G. A solid future for battery development. *Nature Energy* **2016**, *1* (9), 1-4.
(2) Roth, E. P.; Orendorff, C. J. How electrolytes influence battery safety. *The Electrochemical Society Interface* **2012**, *21* (2), 45.
(3) Xu, K. Electrolytes and interphases in Li-ion batteries and beyond. *Chemical reviews* **2014**, *114* (23), 11503-11618.
(4) Chen, R.; Li, Q.; Yu, X.; Chen, L.; Li, H. Approaching practically accessible solid-state batteries: stability issues related to solid electrolytes and interfaces. *Chemical reviews* **2019**, *120* (14), 6820-6877.
(5) Ding, Z.; Li, J.; Li, J.; An, C. Interfaces: Key Issue to Be Solved for All Solid-State Lithium Battery Technologies. *Journal of The Electrochemical Society* **2020**, *167* (7), 070541. DOI: 10.1149/1945-7111/ab7f84.
(6) Lascaud, S.; Perrier, M.; Vallee, A.; Besner, S.; Prud'Homme, J.; Armand, M. Phase diagrams and conductivity behavior of poly (ethylene oxide)-molten salt rubbery electrolytes. *Macromolecules* **1994**, *27* (25), 7469-7477.
(7) Zhang, H.; Hao, S.; Lin, J. Influence of Li2O-B2O3 glass on ionic migration and interfacial properties of La2/3− xLi3xTiO3 solid electrolyte. *Journal of Alloys and Compounds* **2017**, *704*, 109-116.
(8) Meesala, Y.; Jena, A.; Chang, H.; Liu, R.-S. Recent advancements in Li-ion conductors for all-solid-state Li-ion batteries. *ACS Energy Letters* **2017**, *2* (12), 2734-2751.
(9) Kim, K. J.; Balaish, M.; Wadaguchi, M.; Kong, L.; Rupp, J. L. Solid- state Li–metal batteries: challenges and horizons of oxide and sulfide solid electrolytes and their interfaces. *Advanced Energy Materials* **2021**, *11* (1), 2002689.
(10) Keller, M.; Varzi, A.; Passerini, S. Hybrid electrolytes for lithium metal batteries. *Journal of Power Sources* **2018**, *392*, 206-225. DOI: https://doi.org/10.1016/j.jpowsour.2018.04.099.
(11) Isaac, J. A.; Devaux, D.; Bouchet, R. Dense inorganic electrolyte particles as a lever to promote composite electrolyte conductivity. *Nature Materials* **2022**, *21* (12), 1412-1418.
(12) Abe, T.; Sagane, F.; Ohtsuka, M.; Iriyama, Y.; Ogumi, Z. Lithium-Ion Transfer at the Interface Between Lithium-Ion Conductive Ceramic Electrolyte and Liquid Electrolyte-A Key to Enhancing the Rate Capability of Lithium-Ion Batteries. *Journal of The Electrochemical Society* **2005**, *152* (11), A2151. DOI: 10.1149/1.2042907.
(13) Busche, M. R.; Drossel, T.; Leichtweiss, T.; Weber, D. A.; Falk, M.; Schneider, M.; Reich, M.-L.; Sommer, H.; Adelhelm, P.; Janek, J. Dynamic formation of a solid-liquid electrolyte interphase and its consequences for hybrid-battery concepts. *Nature Chemistry* **2016**, *8* (5), 426-434. DOI: 10.1038/nchem.2470.
(14) Sagane, F.; Abe, T.; Iriyama, Y.; Ogumi, Z. Li+ and Na+ transfer through interfaces between inorganic solid electrolytes and polymer or liquid electrolytes. *Journal of Power Sources* **2005**, *146* (1), 749-752. DOI: https://doi.org/10.1016/j.jpowsour.2005.03.075.
(15) Sagane, F.; Abe, T.; Ogumi, Z. Li+-Ion Transfer through the Interface between Li+-Ion Conductive Ceramic Electrolyte and Li+-Ion-Concentrated Propylene Carbonate Solution. *The Journal of Physical Chemistry C* **2009**, *113* (46), 20135-20138. DOI: 10.1021/jp908623c.
(16) Sagane, F.; Miyazaki, K.; Fukutsuka, T.; Iriyama, Y.; Abe, T.; Ogumi, Z. Lithium-ion Transfer at the Interface between Solid and Liquid Electrolytes under Applying DC Voltage. *Chemistry Letters* **2010**, *39* (8), 826-827. DOI: 10.1246/cl.2010.826 (acccessed 2020/08/11).
(17) Schleutker, M.; Bahner, J.; Tsai, C.-L.; Stolten, D.; Korte, C. On the interfacial charge transfer between solid and liquid Li+ electrolytes. *Physical Chemistry Chemical Physics* **2017**, *19* (39), 26596-26605, 10.1039/C7CP05213H. DOI: 10.1039/C7CP05213H.
(18) Uhlmann, C.; Braun, P.; Illig, J.; Weber, A.; Ivers-Tiffée, E. Interface and grain boundary resistance of a lithium lanthanum titanate (Li3xLa2/3−xTiO3, LLTO) solid electrolyte. *Journal of Power Sources* **2016**, *307*, 578-586. DOI: https://doi.org/10.1016/j.jpowsour.2016.01.002.
(19) Yamada, Y.; Sagane, F.; Iriyama, Y.; Abe, T.; Ogumi, Z. Kinetics of Lithium-Ion Transfer at the Interface between Li0.35La0.55TiO3 and Binary Electrolytes. *The Journal of Physical Chemistry C* **2009**, *113* (32), 14528-14532. DOI: 10.1021/jp9043539.

(20) Mehrotra, A.; Ross, P. N.; Srinivasan, V. Quantifying Polarization Losses in an Organic Liquid Electrolyte/Single Ion Conductor Interface. *Journal of The Electrochemical Society* **2014**, *161* (10), A1681-A1690. DOI: 10.1149/2.0721410jes.
(21) Martin R., B.; Thomas, L.; Carsten, F.; Thomas, D.; Matthias, G.; Manuel, W.; Achim, K.; Dominik A., W.; Jürgen, J. *The Formation of the Solid-/Liquid Electrolyte Interphase (SLEI) on NASICON-Type Glass Ceramics and LiPON*; 2020. DOI: 10.26434/chemrxiv.11734740.v1.
(22) Gondran, C.; Albert, F.; Siebert, E. Kinetics of sodium and silver exchange on a PEOx • NaI • (AgI)0.25 based internal reference system. *Solid State Ionics* **1996**, *84* (1), 131-138. DOI: https://doi.org/10.1016/S0167-2738(96)83015-3.
(23) Abe, T.; Ohtsuka, M.; Sagane, F.; Iriyama, Y.; Ogumi, Z. Lithium Ion Transfer at the Interface between Lithium-Ion-Conductive Solid Crystalline Electrolyte and Polymer Electrolyte. *Journal of The Electrochemical Society* **2004**, *151* (11), A1950-A1953. DOI: 10.1149/1.1804813.
(24) Langer, F.; Palagonia, M. S.; Bardenhagen, I.; Glenneberg, J.; La Mantia, F.; Kun, R. Impedance Spectroscopy Analysis of the Lithium Ion Transport through the Li7La3Zr2O12/P(EO)20Li Interface. *Journal of The Electrochemical Society* **2017**, *164* (12), A2298-A2303. DOI: 10.1149/2.0381712jes.
(25) Tenhaeff, W. E.; Yu, X.; Hong, K.; Perry, K. A.; Dudney, N. J. Ionic transport across interfaces of solid glass and polymer electrolytes for lithium ion batteries. *Journal of the Electrochemical Society* **2011**, *158* (10), A1143.
(26) Wang, C.; Yang, Y.; Liu, X.; Zhong, H.; Xu, H.; Xu, Z.; Shao, H.; Ding, F. Suppression of Lithium Dendrite Formation by Using LAGP-PEO (LiTFSI) Composite Solid Electrolyte and Lithium Metal Anode Modified by PEO (LiTFSI) in All-Solid-State Lithium Batteries. *ACS Applied Materials & Interfaces* **2017**, *9* (15), 13694-13702. DOI: 10.1021/acsami.7b00336.
(27) Zhang, T.; Imanishi, N.; Hasegawa, S.; Hirano, A.; Xie, J.; Takeda, Y.; Yamamoto, O.; Sammes, N. Li⁄Polymer Electrolyte⁄Water Stable Lithium-Conducting Glass Ceramics Composite for Lithium–Air Secondary Batteries with an Aqueous Electrolyte. *Journal of The Electrochemical Society* **2008**, *155* (12), A965. DOI: 10.1149/1.2990717.
(28) Brogioli, D.; Langer, F.; Kun, R.; La Mantia, F. Space-Charge Effects at the Li7La3Zr2O12/Poly(ethylene oxide) Interface. *ACS Applied Materials & Interfaces* **2019**, *11* (12), 11999-12007. DOI: 10.1021/acsami.8b19237.
(29) Chen, X. C.; Liu, X.; Samuthira Pandian, A.; Lou, K.; Delnick, F. M.; Dudney, N. J. Determining and minimizing resistance for ion transport at the polymer/ceramic electrolyte interface. *ACS Energy Letters* **2019**, *4* (5), 1080-1085.
(30) Gupta, A.; Sakamoto, J. Controlling Ionic Transport through the PEO-LiTFSI/LLZTO Interface. *The Electrochemical Society Interface* **2019**, *28* (2), 63-69. DOI: 10.1149/2.f06192if.
(31) Weiss, M.; Simon, F. J.; Busche, M. R.; Nakamura, T.; Schröder, D.; Richter, F. H.; Janek, J. From Liquid- to Solid-State Batteries: Ion Transfer Kinetics of Heteroionic Interfaces. *Electrochemical Energy Reviews* **2020**. DOI: 10.1007/s41918-020-00062-7.
(32) Sagane, F.; Abe, T.; Ogumi, Z. Electrochemical analysis of lithium-ion transfer reaction through the interface between ceramic electrolyte and ionic liquids. *Journal of the Electrochemical Society* **2012**, *159* (11), A1766.
(33) Brogioli, D.; Langer, F.; Kun, R.; La Mantia, F. Space-charge effects at the Li7La3Zr2O12/poly (ethylene oxide) interface. *ACS Applied Materials & Interfaces* **2019**, *11* (12), 11999-12007.
(34) Gupta, A.; Sakamoto, J. Controlling ionic transport through the PEO-LiTFSI/LLZTO interface. *The Electrochemical Society Interface* **2019**, *28* (2), 63.
(35) Chinnam, P. R.; Wunder, S. L. Engineered interfaces in hybrid ceramic–polymer electrolytes for use in all-solid-state Li batteries. *ACS Energy Letters* **2017**, *2* (1), 134-138.
(36) Langer, F.; Palagonia, M. S.; Bardenhagen, I.; Glenneberg, J.; La Mantia, F.; Kun, R. Impedance spectroscopy analysis of the lithium ion transport through the Li7La3Zr2O12/P (EO) 20Li interface. *Journal of the Electrochemical Society* **2017**, *164* (12), A2298.
(37) Tenhaeff, W. E.; Perry, K. A.; Dudney, N. J. Impedance Characterization of Li Ion Transport at the Interface between Laminated Ceramic and Polymeric Electrolytes. *Journal of The Electrochemical Society* **2012**, *159* (12), A2118-A2123. DOI: 10.1149/2.063212jes.
(38) Fu, J. Superionic conductivity of glass-ceramics in the system Li 2O-Al 2O 3-TiO 2-P 2O 5. *Solid State Ionics* **1997**, *96* (3-4), 195-200.
(39) corporation, O. *https://www.oharacorp.com/lic-gc.html*. 2010. (accessed.

(40) Lovelock, K. R.; Villar-Garcia, I. J.; Maier, F.; Steinrück, H.-P.; Licence, P. Photoelectron spectroscopy of ionic liquid-based interfaces. *Chemical Reviews* **2010**, *110* (9), 5158-5190.
(41) Isaac, J. A.; Mangani, L. R.; Devaux, D.; Bouchet, R. Electrochemical Impedance Spectroscopy of PEO-LATP Model Multilayers: Ionic Charge Transport and Transfer. *ACS applied materials & interfaces* **2022**, *14* (11), 13158-13168.
(42) Qian, X.; Gu, N.; Cheng, Z.; Yang, X.; Wang, E.; Dong, S. Plasticizer effect on the ionic conductivity of PEO-based polymer electrolyte. *Materials Chemistry and Physics* **2002**, *74* (1), 98-103. DOI: https://doi.org/10.1016/S0254-0584(01)00408-4.
(43) Nithya, H.; Selvasekarapandian, S.; Selvin, P. C.; Kumar, D. A.; Kawamura, J. Effect of propylene carbonate and dimethylformamide on ionic conductivity of P (ECH-EO) based polymer electrolyte. *Electrochimica acta* **2012**, *66*, 110-120.
(44) Kumar, M.; Sekhon, S. Ionic conductance behaviour of plasticized polymer electrolytes containing different plasticizers. *Ionics* **2002**, *8* (3-4), 223-233.
(45) Trinh, N. D.; Lepage, D.; Aymé-Perrot, D.; Badia, A.; Dollé, M.; Rochefort, D. An Artificial Lithium Protective Layer that Enables the Use of Acetonitrile-Based Electrolytes in Lithium Metal Batteries. *Angewandte Chemie International Edition* **2018**, *57* (18), 5072-5075. DOI: https://doi.org/10.1002/anie.201801737.
(46) Rupich, M.; Pitts, L.; Abraham, K. Characterization of reactions and products of the discharge and forced overdischarge of Li/SO 2 cells. *Journal of The Electrochemical Society* **1982**, *129* (9), 1857.
(47) Vivek, J. P.; Meddings, N.; Garcia-Araez, N. Negating the Interfacial Resistance between Solid and Liquid Electrolytes for Next-Generation Lithium Batteries. *ACS Applied Materials & Interfaces* **2021**, *14* (1), 633-646.
(48) Guo, Q.; Xu, F.; Shen, L.; Wang, Z.; Wang, J.; He, H.; Yao, X. Poly (ethylene glycol) brush on Li6. 4La3Zr1. 4Ta0. 6O12 towards intimate interfacial compatibility in composite polymer electrolyte for flexible all-solid-state lithium metal batteries. *Journal of Power Sources* **2021**, *498*, 229934.
(49) Guo, Q.; Xu, F.; Shen, L.; Deng, S.; Wang, Z.; Li, M.; Yao, X. 20 μm-thick Li6. 4La3Zr1. 4Ta0. 6O12-based flexible solid electrolytes for all-solid-state lithium batteries. *Energy Material Advances* **2022**.
(50) Gupta, A. Analyzing the Stability and Kinetics of Ceramic Electrolyte/Organic Electrolyte Interfaces for Li Metal Batteries. Doctoral dissertation, 2020. https://hdl.handle.net/2027.42/163066.
(51) Busche, M. R.; Weiss, M.; Leichtweiss, T.; Fiedler, C.; Drossel, T.; Geiss, M.; Kronenberger, A.; Weber, D. A.; Janek, J. The Formation of the Solid/Liquid Electrolyte Interphase (SLEI) on NASICON- Type Glass Ceramics and LiPON. *Advanced Materials Interfaces* **2020**, *7* (19), 2000380.
(52) Rosen, M.; Ye, R.; Mann, M.; Lobe, S.; Finsterbusch, M.; Guillon, O.; Fattakhova-Rohlfing, D. Controlling the lithium proton exchange of LLZO to enable reproducible processing and performance optimization. *Journal of Materials Chemistry A* **2021**, *9* (8), 4831-4840.
(53) Cella, J. A.; Bacon, S. W. Preparation of dialkyl carbonates via the phase-transfer-catalyzed alkylation of alkali metal carbonate and bicarbonate salts. *The Journal of Organic Chemistry* **1984**, *49* (6), 1122-1125.
(54) Yamada, H.; Takemoto, K. Local structure and composition change at surface of lithium-ion conducting solid electrolyte. *Solid State Ionics* **2016**, *285*, 41-46.
(55) Adachi, G.-y.; Imanaka, N.; Aono, H. Fast Li⊕ Conducting Ceramic Electrolytes. *Advanced Materials* **1996**, *8* (2), 127-135. DOI: https://doi.org/10.1002/adma.19960080205.
(56) Yamada, H.; Tsunoe, D.; Shiraishi, S.; Isomichi, G. Reduced grain boundary resistance by surface modification. *The Journal of Physical Chemistry C* **2015**, *119* (10), 5412-5419.
(57) Ding, D.; Maeyoshi, Y.; Kubota, M.; Wakasugi, J.; Takemoto, K.; Kanamura, K.; Abe, H. Li-ion conducting glass ceramic (LICGC)/reduced graphene oxide sandwich-like structure composite for high-performance lithium-ion batteries. *Journal of Power Sources* **2021**, *500*, 229976.
(58) Castro, L.; Petit, E.; Benayad, A.; Mauvy, F.; Pecquenard, B.; Le Cras, F.; Barchasz, C. Evaluation of chemical stability of conducting ceramics to protect metallic lithium in Li/S batteries. *Solid State Ionics* **2020**, *354*, 115402.
(59) Morales-Ugarte, J. E.; Santini, C. C.; Bouchet, R.; Benayad, A. New Interpretation of X-ray Photoelectron Spectroscopy of Imidazolium Ionic Liquid Electrolytes Based on Ionic Transport

Analyses. *The Journal of Physical Chemistry B* **2020**, *124* (35), 7625-7635. DOI: 10.1021/acs.jpcb.0c04090.
(60) Fiedler, C.; Luerssen, B.; Rohnke, M.; Sann, J.; Janek, J. XPS and SIMS analysis of solid electrolyte interphases on lithium formed by ether-based electrolytes. *Journal of The Electrochemical Society* **2017**, *164* (14), A3742.

TOC

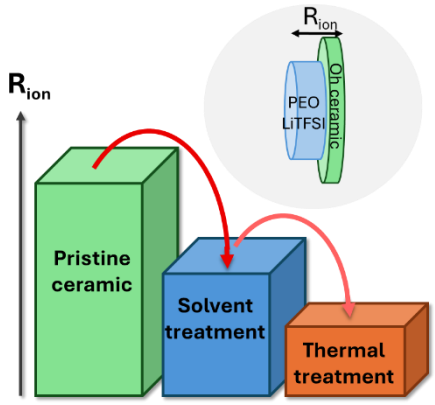
R_ion
R_ion
PEO
LiTFSI
Oh.ceramic
Pristine
ceramic
Solvent
treatment
Thermal
treatment